

Review

Unraveling the Dynamics of SARS-CoV-2 Mutations: Insights from Surface Plasmon Resonance Biosensor Kinetics

Devi Taufiq Nurrohman¹  and Nan-Fu Chiu^{1,2,*} 

¹ Laboratory of Nano-Photonics and Biosensors, Institute of Electro-Optical Engineering, National Taiwan Normal University, Taipei 11677, Taiwan; 81077004h@ntnu.edu.tw

² Department of Life Science, National Taiwan Normal University, Taipei 11677, Taiwan

* Correspondence: nfchiu@ntnu.edu.tw

Abstract: Surface Plasmon Resonance (SPR) technology is known to be a powerful tool for studying biomolecular interactions because it offers real-time and label-free multiparameter analysis with high sensitivity. This article summarizes the results that have been obtained from the use of SPR technology in studying the dynamics of severe acute respiratory syndrome coronavirus 2 (SARS-CoV-2) mutations. This paper will begin by introducing the working principle of SPR and the kinetic parameters of the sensorgram, which include the association rate constant (k_a), dissociation rate constant (k_d), equilibrium association constant (K_A), and equilibrium dissociation constant (K_D). At the end of the paper, we will summarize the kinetic data on the interaction between angiotensin-converting enzyme 2 (ACE2) and SARS-CoV-2 obtained from the results of SPR signal analysis. ACE2 is a material that mediates virus entry. Therefore, understanding the kinetic changes between ACE2 and SARS-CoV-2 caused by the mutation will provide beneficial information for drug discovery, vaccine development, and other therapeutic purposes.

Keywords: COVID-19; surface plasmon resonance; biosensors; kinetics



Citation: Nurrohman, D.T.; Chiu, N.-F. Unraveling the Dynamics of SARS-CoV-2 Mutations: Insights from Surface Plasmon Resonance Biosensor Kinetics. *Biosensors* **2024**, *14*, 99.

<https://doi.org/10.3390/bios14020099>

Received: 23 December 2023

Revised: 8 February 2024

Accepted: 11 February 2024

Published: 13 February 2024



Copyright: © 2024 by the authors. Licensee MDPI, Basel, Switzerland. This article is an open access article distributed under the terms and conditions of the Creative Commons Attribution (CC BY) license (<https://creativecommons.org/licenses/by/4.0/>).

1. Introduction

The global coronavirus disease 2019 (COVID-19) pandemic, caused by the SARS-CoV-2 virus, has resulted in many deaths and severe economic problems in all countries around the world [1–3]. To date, SARS-CoV-2 has mutated thousands of times, and these mutations occur spontaneously during replication [4]. These mutations will have direct implications with the increasing number of new variants of the virus. The bad news is that new variants of SARS-CoV-2 can affect the transmission rate of the virus, the severity of the disease, and the efficacy of the vaccine [5]. The development of sensitive and accurate analytical technology is significant for the purpose of screening and handling viruses that have a high level of spread and transmission that is difficult to avoid. The standard methods have been used to detect COVID-19, including RNA detection by reverse transcription polymerase chain reaction (RT-PCR) from respiratory samples [6], antibody detection by the enzyme-linked immunosorbent assay (ELISA) [7], chest X-rays [8], and computed tomography [9].

Of the several methods mentioned, RT-PCR is still the gold-standard clinical diagnostic method for detecting COVID-19 [10]. Unfortunately, this method requires special equipment with trained personnel. The RT-PCR procedure also takes a long time and has complex steps [11]. Therefore, testing samples in mass quantities is difficult to realize. In this case, methods that are simple, fast, accurate, and sensitive are really needed to deal with the spread of the virus in the future. SPR biosensors have been used for more than 30 years to rapidly and accurately measure several biological and chemical species with very low detection limits at the atto- or femtomolar order [12]. By utilizing surface plasmon waves (SPWs), the interaction between the receptor molecule and the analyte detected can be monitored in real-time by observing the sensorgram signal. This device also offers

parallel analysis through the development of surface plasmon resonance imaging (SPRi) to offer more complete information [13].

Several research groups have reviewed topics related to the use of SPR technology for dealing with COVID-19. For detection, diagnosis, and early screening of SARS-CoV-2, this topic has been reviewed by Pandey's group [14] and Nor's group [15]. More specific topics, such as using SPR technology to find materials that inhibit the entry of SARS-CoV-2 have been reviewed by Mauriz's group [16]. This paper tries to review the different perspectives on the use of SPR in dealing with the COVID-19 pandemic. The main points that will be presented in this paper are illustrated in Figure 1. This paper begins with an introduction to the principles of SPR technology and continues with an introduction to the kinetic parameters of SPR signals. Studies show that the SARS-CoV-2 spike protein will bind to ACE2 to mediate the entry of the virus into cells [17]. Therefore, in the last part of this paper, we will only focus on reviewing kinetic parameters in several cases of SARS-CoV-2 mutation with ACE2. ACE2 is the main natural receptor that mediates viral entry, and therefore, no modification of ACE2 is required in studying the kinetic parameters of different mutation and variants of SARS-CoV-2 [18]. Furthermore, information related to kinetic parameters will be useful in monitoring epidemiological developments, vaccine development, drug discovery, and so on [16,19].

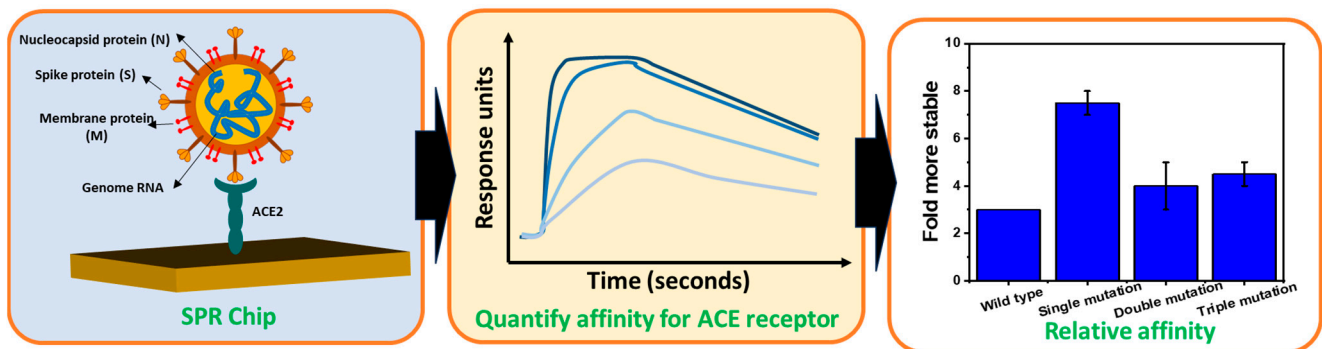


Figure 1. Schematic diagram to illustrate the contents of this paper.

2. Working Principle and Development of a Prism-Based SPR Biosensor

The SPR biosensor is one type of biosensor that utilizes surface plasmon waves in its work. Surface plasmon waves are generated when light interacts with free electrons at the interface between a metal (or other conducting material) and a dielectric (usually glass, air, or liquid) [20]. When monochromatic light with p-polarization strikes a metal surface, the light will be absorbed by electrons and cause collective oscillations of electrons called plasmons [21]. Surface plasmon waves propagate on metal and dielectric surfaces with a wave number symbolized by k_{sp} and its magnitude can be determined mathematically using the following equation [22]:

$$k_{sp} = \frac{\omega}{c} \sqrt{\frac{(\epsilon_m \epsilon_d)}{(\epsilon_m + \epsilon_d)}}, \quad (1)$$

where ω is the frequency of incident light, c is the speed of light, ϵ_m and ϵ_d are the dielectric constants of the metal and the dielectric, respectively. Because the dielectric constant is related to the refractive index (n) based on the relationship $\sqrt{\epsilon_{real}}$ [23], then k_{SP} in Equation (1) can be modified to [24]:

$$k_{sp} = \frac{\omega}{c} \sqrt{\frac{(n_m^2 n_d^2)}{(n_m^2 + n_d^2)}}, \quad (2)$$

where n_m and n_d indicate the refractive index of the metal and the dielectric.

If we measure the intensity of reflected light, at a certain angle of incidence we will find an angle where the light will show a very low intensity. This happens because the incident light is completely absorbed by the electrons. The angle at which the intensity of the reflected light shows the smallest intensity is usually called the SPR angle or the resonance angle. The resonance condition occurs when the wave number of the photon is equal to the wave number of the surface plasmon. This can be explained using a dispersion curve as shown in Figure 2a. Surface plasmon waves cannot be excited by direct light because the wave vector of the surface plasmon is higher than the incident light. The wave vector of the surface plasmon (blue curve) will never intersect with the wave vector of the photon (red curve) over the entire wave number range. To achieve resonance conditions, the dispersion curve of the surface plasmon must be reduced or the dispersion curve of the photons increased. One widely used approach is to add a prism with a high refractive index to increase the photon dispersion curve. By adding a prism, the photon wavenumber changes from

$$k_x = \frac{\omega}{c} \sin \theta \tag{3}$$

to

$$k_x = \frac{\omega}{c} n_p \sin \theta. \tag{4}$$

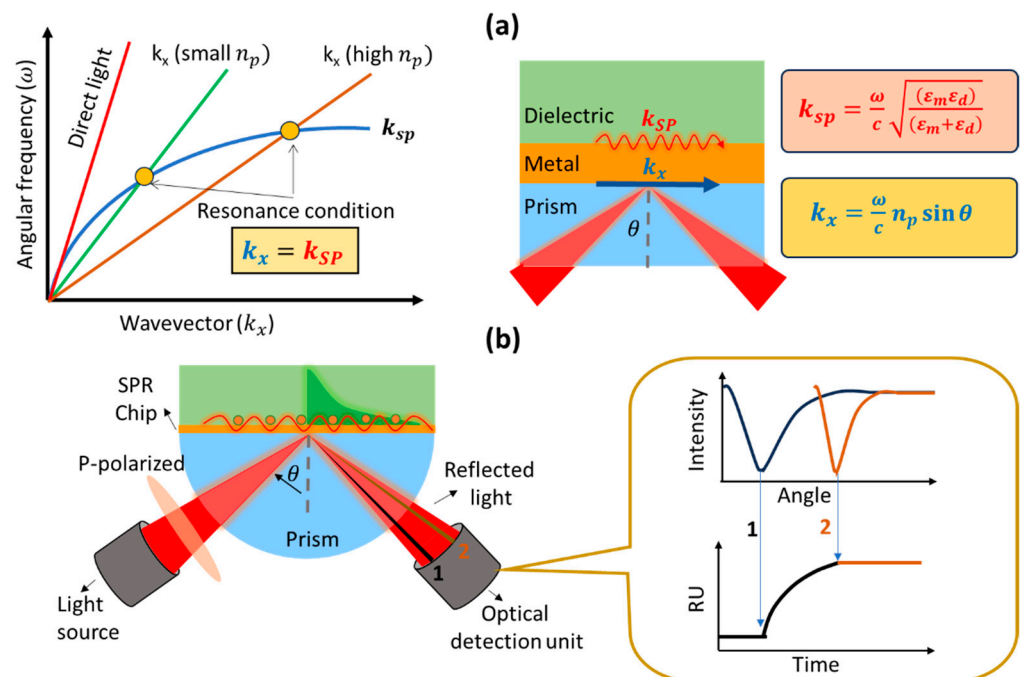


Figure 2. (a) Surface plasmon dispersion curve. (b) Schematic of the prism-coupled SPR biosensor and the resulting signal.

Since the refractive index of the prism is constant, the resonance angle will depend on the presence or absence of adsorbed molecules at the metal and dielectric interfaces on the sensing surface. The presence of adsorbed molecules will result in a shift in the resonance angle. Therefore, we can monitor the presence or absence of adsorbed molecules or find out how fast the molecules are absorbed (kinetic analysis) from the SPR sensorgram (Figure 2b). There are several parameters that we can obtain from the SPR sensorgram, which are the association rate constant (k_a), dissociation rate constant (k_d), equilibrium association constant (K_A), and equilibrium dissociation constant (K_D). All these quantities will be discussed in the next section.

In 1982, SPR technology was used for gas detection. SPR technology continues to be developed for wider applications such as food safety [25], environmental monitor-

ing [26], medical diagnosis and detection [27], drug discovery [14], and others. Apart from these, another focus in the development of SPR biosensors is on transducer engineering to achieve sensitive sensors so that analytes can be detected down to the smallest possible concentration. By modifying the SPR chip using 2D materials such as graphene and MoS₂, various biomarkers with very small concentrations can be detected. Chiu et al. modified the surface of a thin layer of gold on an SPR chip with graphene oxide to detect human chorionic gonadotropin (hCG) proteins [28]. The detection limit that can be achieved by this sensor system is 0.065 nM, and when compared with conventional SPR biosensors, modification with graphene oxide can increase the sensitivity of the biosensor up to 16 times higher. In 2021, Chiu et al. also modified the SPR chip using MoS₂ to detect pregnancy-associated plasma protein-A2 (PAPP-A2) [29]. The detection limit obtained was 0.05 pg/mL with a linear range of detection ranging from 0.1 to 1100 pg/mL.

3. Principle of SPR Kinetics

An SPR biosensor is a potential tool which can be used to investigate phenomena that occur on the sensing surface. Surface phenomena such as molecular absorption cause changes in the refractive index and change the SPR angle. The SPR angle will shift to a higher angle when a molecule is adsorbed and will shift to a smaller angle when a molecule is released from the sensing surface. The response of the SPR biosensor due to a phenomenon on the sensing surface can be plotted at any time in real-time, and the resulting curve is called a sensorgram curve. Kinetic parameters that describe bonding events can be obtained, such as the association, dissociation, and equilibrium constants [30].

In the simplest SPR experiment, the experiment begins with the immobilization of the active ligand to specifically recognize the molecule to be detected (Figure 3a). Ligands can be immobilized on the sensor surface through a material that is usually called self-assembled monolayers (SAM) [31]. The target molecule to be detected in this case is called the analyte. The buffer that flows over the sensor surface is called the running buffer [32]. It is essential to condition the sensor surface with an appropriate buffer solution, and the types of buffers that are widely used in SPR experiments are HEPES, Tris, or PBS [33].

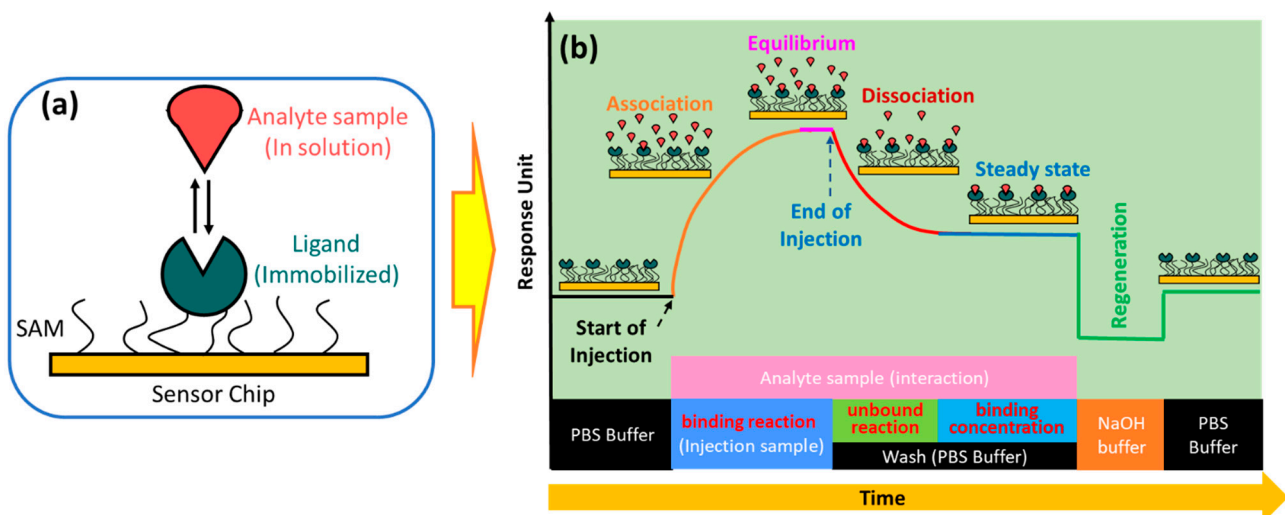


Figure 3. (a) Biosensor chip architecture; (b) SPR sensorgram at different phase.

As shown in Figure 3b, the capture of the analyte by the ligand begins with the conditioning of the running buffer signal. The signal on the sensorgram must form a stable baseline. External influences that cause signal fluctuations in the sensorgram, such as temperature, must be minimized to be as small as possible [34]. Once a baseline is obtained, the solution containing the analyte can be injected. Ligands immobilized on the sensor surface will capture the analyte, and this is indicated by an increase in the sensorgram signal. The magnitude of the sensorgram signal increase depends on the number of active

ligands. After the active ligand pairs with the analyte, the sensorgram signal will be in an equilibrium state. This phase is called the association phase. In the same phase, non-specific interactions caused by the presence of impurities in the analyte solution are also very likely to occur. Therefore, washing is carried out using a running buffer. The remaining analytes and components that are not tightly bound will be removed from the sensor surface. This phase is called the dissociation phase. After this phase has been successfully completed, the sensorgram signal will show a steady state. Finally, the regeneration solution is injected into the sensing surface to break the bond between the analyte and the ligand. If the ligands are immobilized properly, all ligands will remain on the sensing surface, and measurements for other analyte samples can be made using the same SPR chip [30,35–37]. SPR biosensors are usually equipped with two channels: where the first channel is used to obtain a sensorgram signal from the analyte, and the other channel is used to obtain a reference sensorgram signal. The actual signal is obtained after correction by subtracting the measured analyte signal from the reference signal [38,39].

If the ligand on the sensing surface is symbolized by B is bonded to the analyte symbolized by A , the bond between them produces a complex molecule symbolized by AB . The interaction can be written by the following equation [37]:



The association rate constant is defined as the number of complex molecules formed per unit time at concentrations of A and B . This quantity is usually denoted by k_a and in some references it is denoted by k_{on} . Furthermore, the dissociation rate constant indicates the number of complex molecules that decay over time. This quantity is usually symbolized by k_d and in some references it is written as k_{off} . Equilibrium is reached when the rates of association and dissociation are equal. The association and dissociation equilibrium constants represent the affinity of the interaction between ligand and analyte. The affinity of the molecule for association is expressed by K_A . The last one is K_D . This quantity indicates the stability of the formation of the AB complex molecule where a high K_D value indicates the low stability of the formation or interaction of the A and B molecules [40]. Table 1 below shows the definitions, units, and typical ranges for k_a , k_d , K_A , and K_D .

Table 1. Definition, units, and typical range of k_a , and K_D .

	k_a	k_d	K_A	K_D
Definition	$A + B \rightarrow AB$	$AB \rightarrow A + B$	$\frac{[AB]}{[A][B]} = \frac{k_a}{k_d}$	$\frac{[A][B]}{[AB]} = \frac{k_d}{k_a}$
Unit	$\frac{L}{mol \cdot s}$	s^{-1}	L/mol	mol/L
Typical range	$10^3 - 10^7$	$10^{-1} - 5 \times 10^{-6}$	$10^5 - 10^{12}$	$10^{-5} - 10^{-12}$

To produce a good sensorgram signal, there are a few tips to consider. Some of them are related to pH and the type of buffer used, the reactive group, and the molecular weight. The reactive group is important because it ensures covalent coupling of the ligands on the sensor surface. Ligands must contain reactive groups such as $-NH_2$, $-SH$, or $-COOH$ to capture proteins and oligonucleotides. Molecular weight will affect the signal that will be generated, where smaller molecules can change the refractive index to be lower than that of

larger molecules. In many cases, researchers usually immobilize a molecule with a smaller molecular weight as a ligand to obtain a higher signal [41]. The relationship between the molecular weight of the analyte ($MW_{analyte}$), ligand (MW_{ligand}), and the ligand response (R_{ligand}) with the binding capacity of the analyte is shown in the following equation [42]:

$$\text{Analyte binding capacity (RU)} = \frac{MW_{analyte}}{MW_{ligand}} \times R_{ligand}(\text{RU}) \quad (6)$$

The response to the binding capacity of the molecule is only maximal when the ligand on the sensing surface is fully active. However, in many experiments, some ligands on the sensing surface are not active, so the signal response obtained is smaller.

4. COVID-19 Virus and Its Mutation

The SARS-CoV-2 virus is a member of the betacoronavirus genus and has a genome similar to that of SARS-CoV (about 80%) and Middle East respiratory syndrome coronavirus (MERS) (about 50%) [43]. In simple terms, this virus has a spherical shape with a diameter of 130 nm and is surrounded by a spike-like structure on its entire surface, as shown in Figure 4. This virus encodes sixteen non-structural proteins (NSPs) and four structural proteins, which are the nucleocapsid protein (NP), spike glycoprotein (SP), membrane protein (MP), and envelope protein (EP) [44]. The SP is composed of an N-terminal S1 subunit and a C-terminal S2 subunit located near the membrane [45]. The S1 subunit contains RBD, which can bind to ACE2 as a cellular receptor during virus entry, and after that, the Transmembrane domain in subunit S2 will help the virus enter the host cell [44,45].

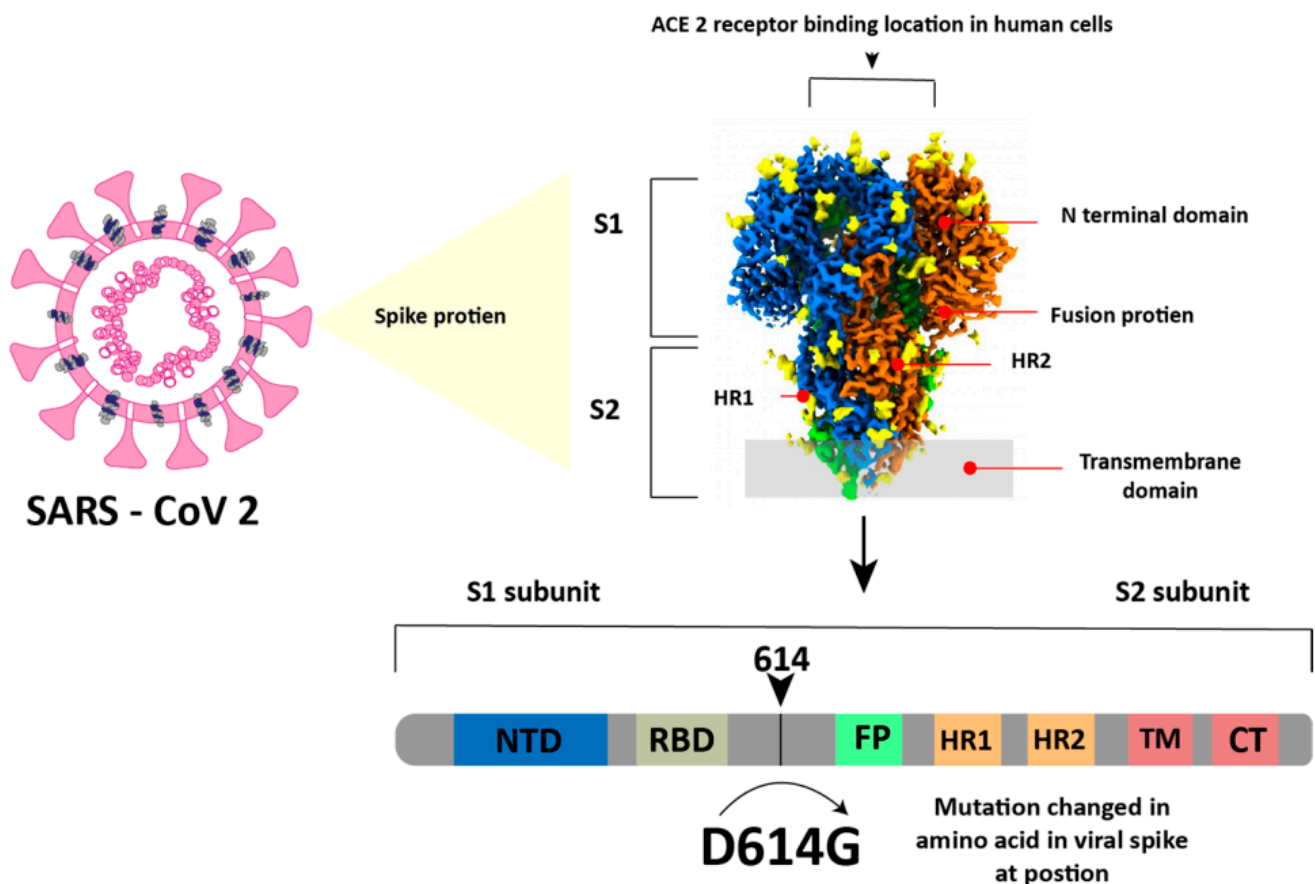


Figure 4. Structure of the SARS-CoV-2 virus. Reproduced with permission from [45]. Copyright (2023), Springer.

SARS-CoV-2 continues to evolve over time. These changes can affect the characteristics of the virus, such as changes in the speed of its spread. Since it was first identified in December 2019 to November 2021, SARS-CoV2 has mutated five times with variants called alpha B.1.1.7 in September 2020, beta 1.351 in October 2020, gamma P.1 in November 2020, delta B.1.617.2 in December 2020, and the last one is Omicron B.1.1.529 in November 2021. Before the discussion continues, it is very important to know the difference between a mutation and a variant to make the discussion clearer and to avoid misunderstanding. Mutations are defined as amino acid exchanges (nonsynonymous or missense) in spike glycoproteins, while other nucleotide changes (synonymous or non-missense) are defined as variants [46,47]. One of the most significant mutations in SARS-CoV-2 is the D614G mutation (Figure 4). In the D614G mutation type, the amino acid aspartate (D) at position 614 in the viral spike protein is replaced by the amino acid glycine (G) [48,49].

Mutations in the SARS-CoV-2 virus can occur in various positions in the viral genome. The SARS-CoV-2 genome is a long RNA chain, and mutations can occur in the spike protein, RBD, N-Terminal Domain (NTD) and others. The complete amino acid changes that occur as a result of the mutations are shown in Figure 5, and to illustrate the differences between each variant, we compared them to the structure of the ancestral protein. In addition, RBD is a part of the S protein that interacts directly with the ACE2 receptor in human cells. Mutations in the RBD can affect the virus' ability to bind to human cells. Therefore, we show the mutations that occur in the RBD which are shown in Table 2.

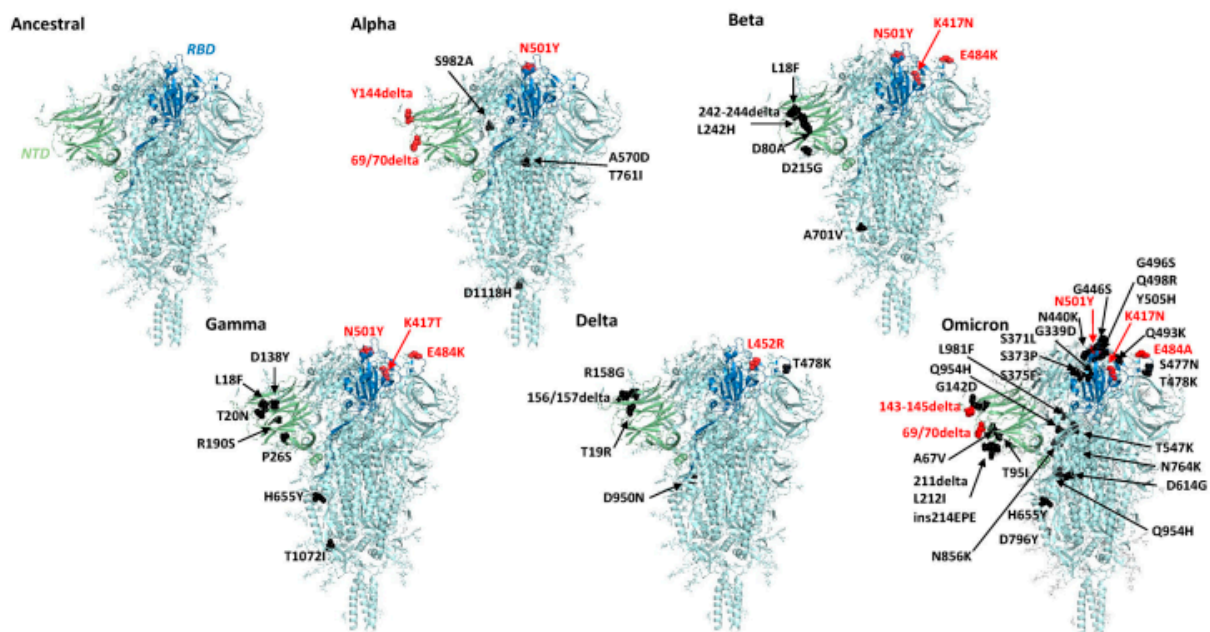


Figure 5. 3D structure of the spike protein of SARS-CoV-2 variants alpha, beta, gamma, delta, and omicron in comparison with an ancestral virus. Reproduced with permission from [50]. Copyright (2023), mBio.

Table 2. Variants of concerns' lineages, and the location of their mutations on the RBD [51].

Variants	Lineage	Mutations on the RBD
Alpha	B.1.1.7	N501Y
Beta	B.1.351	K417N, E484K, N501Y
Gamma	P.1	K417T/N, E484K, N501Y
Delta	B.1.617.2	L452R, T478K
Omicron	B.1.1.529	G339D, S371L, S373P, S375F, K417N, N440K, G446S, S477N, T478K, E484A, Q493R, G496S, Q498R, N501Y, Y505H

5. Application of SPR Technology for SARS-CoV-2 Detection and Analysis of Its Binding

Biosensors are detection devices that use ligands as molecular recognition elements to detect the target molecule specifically. In the context of detecting the COVID-19 virus, several materials can be used as ligands, such as ACE2 [52], monoclonal antibodies (Mabs) [53], aptamers [54], peptides [55], and immunoglobulin molecules (IgM/IgG) [56]. Table 3 below summarizes the various nanophotonic biosensors that have been developed, and to illustrate sensor performance, we include the limit of detection (LoD) obtained from each sensor.

Table 3. Representative paper for nanophotonic biosensors for detecting SARS-CoV-2.

Optical Effect	Ligands	Analytes	LoD	Ref.
SERS	ACE2	SARS-CoV-2 S Protein	0.1 fg/mL	[57]
LSPR	Aptamer	SRBD and SARS-CoV-2 pseudovirus	21.9 pM	[58]
SPR	anti-SARS-CoV-2 spike S1 protein	S1 protein	12 fg/mL	[59]
SPR	anti-SARS-CoV-2 spike MAbs	SARS-CoV-2 spike antigen	0.08 pg/mL	[60]
Fiber optics	ACE2	SARS-CoV-2 spike protein	~3.05 ng/mL	[61]
SERS	SARS-CoV-2 spike antibody	Spike protein	0.77 fg/mL	[62]
SERRS	SARS-CoV-2 antibodies	SARS-CoV-2 spike glycoprotein (S1)	0.60 pM	[63]
BLI	ACE2	S protein	500 pg/mL	[52]
Fiber optics	single-stranded DNA (ssDNA) aptamer	SARS-CoV-2 Nucleocapsid Protein	2.8 nM	[64]

Note: SERRS: Surface-enhanced Resonance Raman scattering; BLI: Biolayer interferometry.

Of the ligands mentioned above, ACE2 is a type of ligand that is widely used to detect the SARS-CoV-2 virus. ACE2 is a natural receptor that is available in various tissues in the human body, especially in cells in the respiratory tract (highest in the olfactory bulbs) [65]. SARS-CoV-2 uses the spike protein on its surface to bind to the ACE2 receptor on human cells. By utilizing this type of ligand, the binding affinity of different variants of SARS-CoV-2 resulting from mutations can be analyzed and identified based on changes in their kinetic parameters. This information is very important not only in virus detection, but also in vaccine development and drug discovery.

Although ACE2 has been identified as the main receptor that mediates entry of the SARS-CoV-2 virus into human cells, heparan sulfate has been identified as a molecule that plays a role in the early stages of viral infection in host cells. A comparison of the affinity between heparin and ACE2 with spike protein has been investigated previously by Liu et al. [66]. They started the experiment by immobilizing heparin and ACE2 on the surface of a streptavidin chip. After that, the K_D value was determined on three different protein samples, namely RBD, spike monomer, and spike trimmer. The analysis results show that the K_D value of the interaction between ACE is always smaller than heparin. In the case of the RBD protein, the K_D values for the heparin chip and ACE2 were ~1000 nM and 3.6 nM, respectively. These results confirm that the RBD domain has a much higher affinity for ACE2 compared with heparin.

Previous results showed that the affinity of ACE2 was much higher than that of heparin. Therefore, Wrapp et al. used ACE2 and compared k_a , k_d , and K_D on two different samples which were s-proteins of the novel coronavirus (2019-nCoV) and the RBD sub-domain 1 (SD1) of SARS-CoV. Serial dissolution of ACE2 was carried out to obtain a 1:1 binding stoichiometry. After ACE2 injection, a sensorgram for each concentration of ACE2 was obtained, as shown in Figure 6. The black line shows the real data while the red line shows the fitting data. If we compare the K_D value of 2019-nCoV S and SARS-CoV RBD-SD1, the K_D value of SARS-CoV RBD-SD1 shows a much higher value of 325.8 nM. As explained in the previous section, a high K_D value indicates a low stability in the formation of bonds between the two molecules. Therefore, it can be concluded that 2019-nCoV S has a higher affinity, which is 20 times higher than the binding between ACE2 and SARS-CoV RBD-SD1 [67].

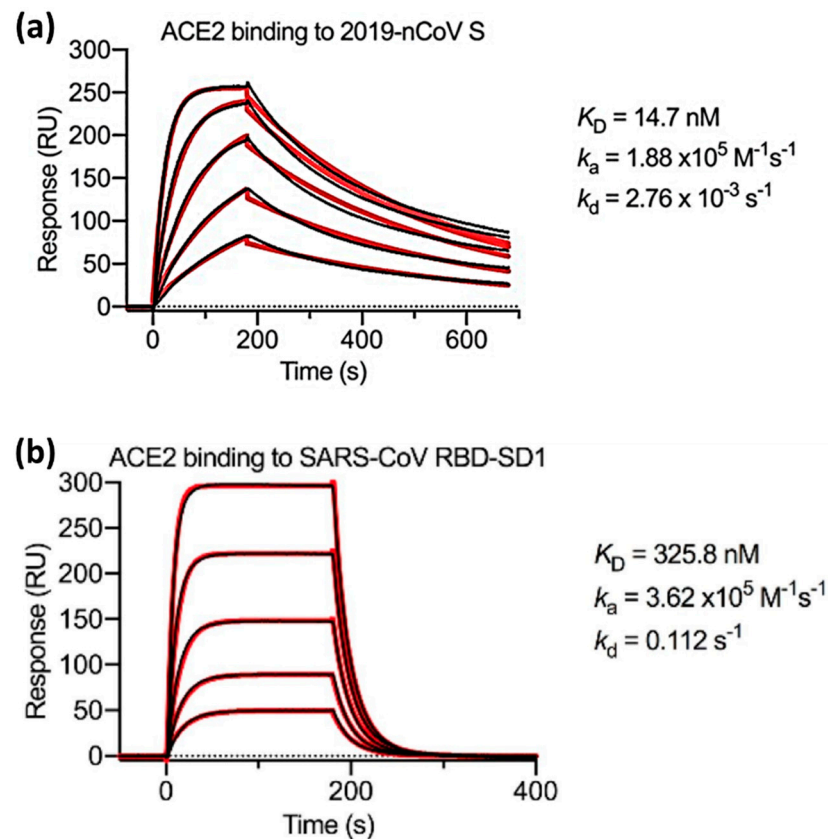


Figure 6. SPR sensorgram showing kinetic binding for ACE2 with (a) 2019-nCoV S, (b) SARS-CoV RBD-SD1. Reproduced with permission from [67]. Copyright (2020), Science.

In the same year, Lan et al. also compared the binding affinity between SARS-CoV-2 RBD and SARS-CoV RBD. ACE2 was employed as a ligand and immobilized on the CM5 chip sensor surface. The response generated after ACE2 injection is 500 response units. Serial dilution was carried out on samples of SARS-CoV-2 RBD and SARS-CoV RBD to obtain a 1:1 bonding model using Biocore Insight Software evaluation software (GE Healthcare, Massachusetts, United States) and the concentrations obtained were in the range of 1.95 nM to 62.5 nM. Figure 7 shows a sensorgram for this concentration range where the K_D values of SARS-CoV-2 RBD and SARS-CoV RBD were 4.7 nM and 31 nM, respectively [43]. Walls et al. in 2020 conducted a kinetic analysis between human ACE2 (hACE2) with SARS-CoV-2 S and SARS-CoV S using a biosensor based on biolayer interferometry (BLI). The results obtained showed that the K_D values of SARS-CoV-2 S and SARS-CoV S were 1.2 nM and 5 nM, respectively [68]. If we compare some of the results above, the K_D values obtained show a slightly different magnitude, but both have similarities, namely the K_D of SARS-CoV-2 S is always smaller than that of SARS-CoV S. The conclusion from our discussion above shows that the kinetic data prove that SARS-CoV-2 S has a higher binding affinity to the ACE2 receptor.

To date, the SPR biosensor has been proven to be able to be used to identify mutation phenomena in the SARS-CoV-2 protein. The effect of D614G on the kinetic parameters of SARS-CoV-2 S proteins and ACE2 has been successfully investigated by Yurkovetskiy et al. [69]. In this research the SPR biosensor was designed to distinguish between G614 and D614. A comparison of kinetic parameters between the SARS-CoV-2 D614G S protein and the ancestral protein was also carried out. The results of this study indicate that the detected RBD mutation has a correlation with SARS-CoV-2 infectivity. The SARS-CoV-2 variant that continues to mutate causes the infectivity of the virus to enter the body to be higher. Several studies have reported changes in the binding affinity of ACE2 after the virus mutates [49]. Xue et al. investigated nine different mutations and compared them with wild

type (WT). The mutants investigated were Q498W, Q498R, T500W, S477H, Y505W, T500R, N501V, Y489W, and Q493M [70]. The K_D value of WT is 21.08 nM. Of the nine mutants investigated, three of them had higher K_D values, namely T500W ($K_D = 21.8$ nM), N501V ($K_D = 158.50$ nM), and Y489W ($K_D = 38.90$ nM). Since most of the K_D s decreased after mutation (the smallest K_D was Q493M (6.9 nM)), this indicates that the presence of viral mutations could strengthen the binding affinity.

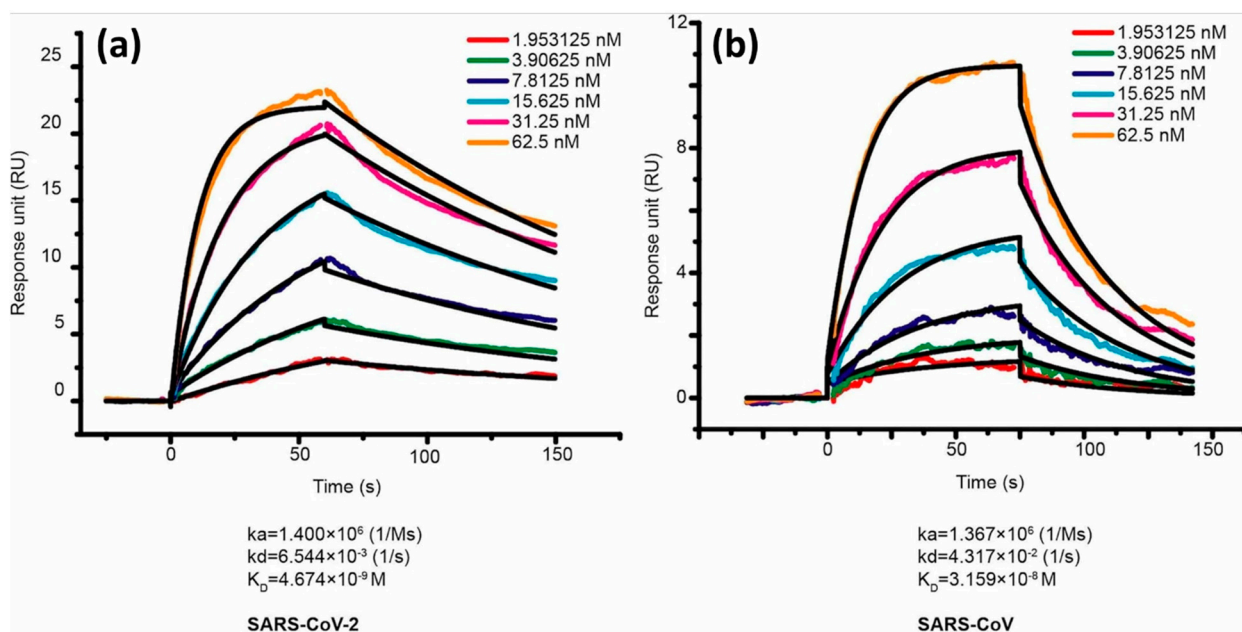


Figure 7. Binding curves of immobilized human ACE2 with the SARS-CoV-2 RBD (a) and SARS-CoV RBD (b). Reproduced with permission from [43]. Copyright (2020), Nature.

The effect of mutations was also investigated by Barton et al. in 2021 [71]. They investigated the affinity and kinetics of five types of RBD mutations (K417N, K417T, N501Y, E484K, and S477N) and two ACE2 mutations (S19P and K26R). Then, they compared it with WT RBD (In Figure 8, the affinity and kinetics of WT RBD are shown by dashed lines). As shown in Figure 8a, the RBD mutation increased binding to the single mutations (S477N, E484K, and N501Y). Of these three single-mutation types, N501Y showed the highest increase, which was 10 times higher than WT RBD. Not only single mutations, but also double (E484K/N501Y) and triple mutations (K417N/E484K/N501Y and K417T/E484K/N501Y) have higher affinity than RBD WT. The same results also occur in ACE2 mutations. Of the two types of ACE2 mutations investigated, both increased the binding affinity between ACE2 and RBD.

Not only can changes in the binding affinity parameters of the SARS-CoV-2 virus caused by mutations be predicted through experimental studies, but they can also be predicted through computational studies. Various approaches to this problem have been developed, including Free Energy Perturbation (FEP) [72,73], machine learning [74], statistical potentials [75], and various force field-related scoring functions embedded in programs such as FoldX [76] and Rosetta [77]. Sergeeva et al. investigated the effect of mutations on the binding affinity of ACE2 with SARS-CoV-2 using FEP [78]. In this study, they investigated the binding affinity (K_D) of ACE2 with wild type (WT) and 23 single mutants. In addition, the epistatic effect of the Q498R N501Y double mutant on the omicron variant can also be determined accurately. These computational results have been successfully confirmed based on SPR experiments.

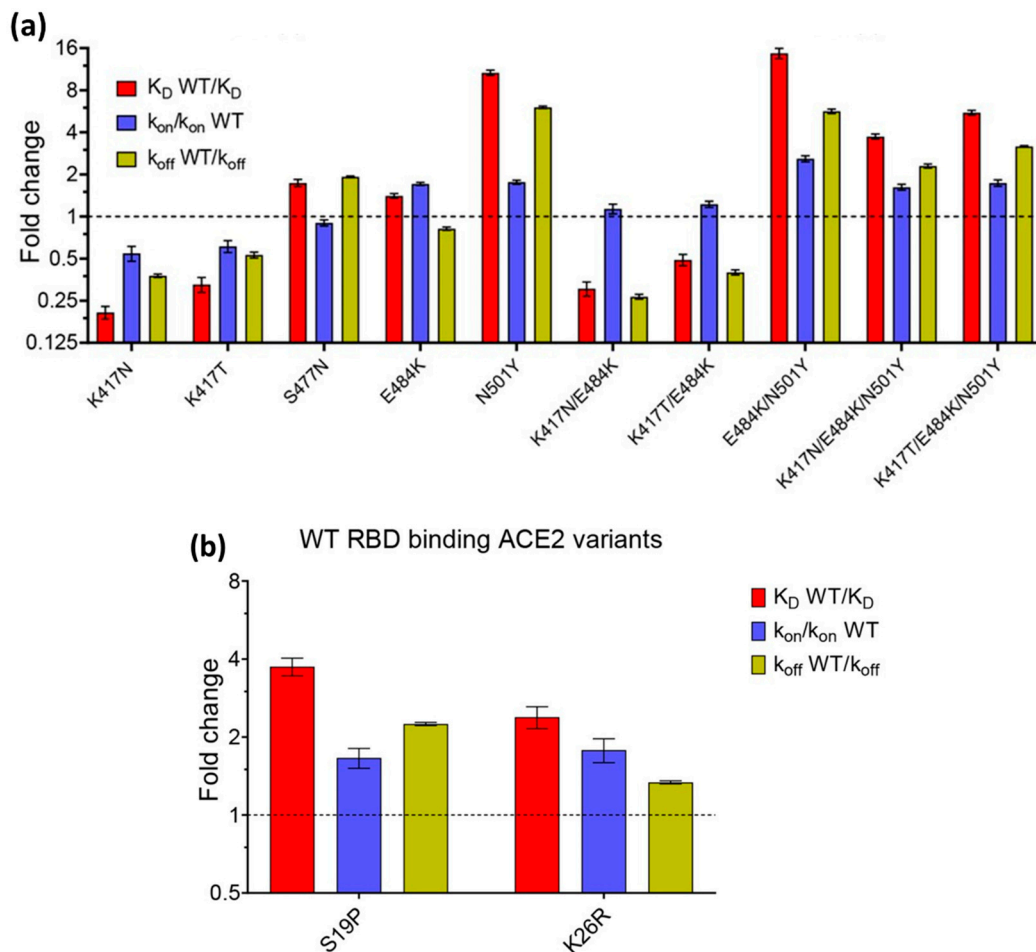


Figure 8. Kinetic parameters (k_a , k_d , and K_D) due to (a) RBD mutation and (b) ACE2 mutation. Reproduced with permission from [71]. Copyright (2020), eLife.

Makowski and his colleagues have analyzed the mutational variations in SARS-CoV-2 against ACE2 using a computational approach supported by machine learning [79]. In this study, it was found that the affinity (K_A) of the beta (RBD Mutations: K417N, E484K, N501Y) and gamma (RBD Mutations: K417T, E484K, N501Y) variants tended to maintain their affinity level compared to the wild type (WT), remaining at around 1×10^{11} M. However, the affinity (K_A) of the alpha (RBD Mutation: N501Y), epsilon (RBD Mutation: L452R), and delta (RBD Mutation: L452R, T478K) variants experienced a significant increase, reaching 1.48×10^{11} M for the alpha variant, 2.54×10^{11} M for the epsilon, and 4.37×10^{11} M for the delta variant. This study also investigated the individual impact of 15 RBD mutations on ACE2 affinity. It was found that five RBD mutations (G339D, N440K, S477N, T478K, and N501Y) increased the affinity of ACE2. In addition, most RBD mutations are also predicted to increase antibody release, with the E484A mutation shown to substantially decrease the neutralization activity of human convalescent serum.

Affinity is information that refers to the strength of an interaction between a particular molecular target and a receptor in a human cell. From the references discussed above, changes in the structure of the virus and the mutations that occur result in changes in its binding affinity. Understanding these affinity changes is critical for controlling viral transmission, vaccination strategies, and future drug development. In the context of biosensors, machine learning is not only used to obtain affinity data from SPR biosensors. Machine learning has also been utilized in studying different nonlinear optical effects. The combination of machine learning analysis tools and multiphotonic effects has enormous potential in data interpretation. Gupta et al. used Principal Component Analysis (PCA)

as a learning machine to improve SERS signals [80]. The use of PCA in this research was able to increase the SERS signal to be up to three times higher. Other researchers, namely Paryanti et al. [81] and Williamson et al. [82], use a different algorithm which is Neural Networks. Details regarding the use of machine learning in nonlinear optical effects are discussed in the following paper [83].

Martinez et al. summarize the process in machine learning into several parts [83]. After the biosensor data are acquired, the raw data obtained are first processed through data filtering and segmentation. Furthermore, normalization is also carried out at this stage to homogenize the scale or data type according to the data's properties. After that, the appropriate model must be determined and this depends on the problem being analyzed and the characteristics of the data being analyzed. There are three models that can be used, namely classification, regression, and clustering. After the model is selected, model learning and evaluation is carried out. Once the selected model is valid and successfully implemented, regular monitoring and maintenance is required to update the algorithm according to changes within the data or environment. In this way, hidden patterns of complex biological systems such as SARS-CoV-2 mutations can be recognized with the help of computing systems in machine learning. The use of machine learning in analyzing biosensor data will be very important in dealing with future pandemics.

6. Conclusions and Future Prospective

The global COVID-19 epidemic has become a major threat to public health worldwide. Thousands of mutations have been identified in the SARS-CoV-2 genome. This paper was written to summarize the dynamics of SARS-CoV-2 mutations using SPR biosensors. The main advantage of SPR biosensors is their ability to offer real-time monitoring of molecular interactions. This property is very important, especially in the case of studying the structure and dynamics of viruses. From the information previously described, we know how the interaction affinity between ACE2 and SARS-CoV-2 changes, both wild type and mutated. Deep insights into interaction dynamics can be explored in more depth by analyzing levels of association and dissociation.

SPR biosensor is a type of label-free biosensor. The absence of labels (e.g., fluorophores) minimizes the complexity in the sample preparation and the risk of contamination. The analysis process becomes faster, and the measured signal is a real signal that represents the properties of the analyte itself. The progress that has been achieved to date is that SPR biosensors can be used to detect analytes up to the atto order. Another advantage of the SPR biosensor is that the transducer is also compatible for use simultaneously with other biosensors. As a result, it is possible to obtain dual mode sensor. Regarding the dual mode biosensor, the SPR biosensor has been successfully integrated with electrochemical [84], surface-enhanced Raman scattering (SERS) [85], electrolyte-gated field-effect transistor (EG-FET) [86].

From the advantages mentioned above, currently existing biosensors, especially SPR biosensors coupled to prisms, are still bulky in size. Therefore, to obtain a more compact and portable device, several research groups are developing fiber-optic-based SPR biosensors. To obtain better sensitivity and lower detection limit, several structures have been developed such as single-mode optical fibers (unclad, side-polished, tapered, and U-shaped), long period fiber gratings (LPFG), tilted fiber Bragg gratings (TFBG), and specialty fibers (plastic or polymer, microstructured, and photonic crystal fibers) [87]. Furthermore, to simultaneously detect several targets or biomarkers in one test, multiplex biosensors need to be developed. This is very important to obtain more comprehensive data. By combining multiplexing capabilities with high detection sensitivity, multiplex biosensors enable more effective monitoring of new variants and mutations that may emerge over time.

Author Contributions: D.T.N.: investigation, data curation, writing—original draft. N.-F.C.: conceptualization, methodology, data curation, supervision, data curation, investigation, resources, methodology. All the authors contributed equally and have given approval to the final version of the manuscript. All authors have read and agreed to the published version of the manuscript.

Funding: This study was funded by the Ministry of Science and Technology of the Republic of China (ROC), Taiwan, for financially supporting this research under Contract No. MOST 108-2221-E-003-020-MY3, MOST 109-2221-E-003-028-MY3, NSTC 112-2221-E-003-016-MY3. This work is sponsored by “Higher Education Sprout Project” of National Taiwan Normal University and the Ministry of Education (MOE) in Taiwan.

Institutional Review Board Statement: Not applicable.

Informed Consent Statement: Not applicable.

Data Availability Statement: Not applicable.

Conflicts of Interest: The authors declare no conflicts of interest.

References

1. Ciotti, M.; Angeletti, S.; Minieri, M.; Giovannetti, M.; Benvenuto, D.; Pascarella, S.; Sagnelli, C.; Bianchi, M.; Bernardini, S.; Ciccozzi, M. COVID-19 Outbreak: An Overview. *Chemotherapy* **2020**, *64*, 215–223. [[CrossRef](#)]
2. Hui, D.S.; I Azhar, E.; Madani, T.A.; Ntoumi, F.; Kock, R.; Dar, O.; Ippolito, G.; Mchugh, T.D.; Memish, Z.A.; Drosten, C.; et al. The Continuing 2019-NCov Epidemic Threat of Novel Coronaviruses to Global Health—The Latest 2019 Novel Coronavirus Outbreak in Wuhan, China. *Int. J. Infect. Dis.* **2020**, *91*, 264–266. [[CrossRef](#)]
3. Wu, J.T.; Leung, K.; Leung, G.M. Nowcasting and Forecasting the Potential Domestic and International Spread of the 2019-NCov Outbreak Originating in Wuhan, China: A Modelling Study. *Lancet* **2020**, *395*, 689–697. [[CrossRef](#)]
4. Cosar, B.; Karagulleoglu, Z.Y.; Unal, S.; Ince, A.T.; Uncuoglu, D.B.; Tuncer, G.; Kilinc, B.R.; Ozkan, Y.E.; Ozkoc, H.C.; Demir, I.N.; et al. SARS-CoV-2 Mutations and Their Viral Variants. *Cytokine Growth Factor Rev.* **2022**, *63*, 10–22. [[CrossRef](#)]
5. He, C.; Lin, C.; Mo, G.; Xi, B.; Li, A.; Huang, D.; Wan, Y.; Chen, F.; Liang, Y.; Zuo, Q.; et al. Rapid and Accurate Detection of SARS-CoV-2 Mutations Using a Cas12a-Based Sensing Platform. *Biosens. Bioelectron.* **2022**, *198*, 113857. [[CrossRef](#)] [[PubMed](#)]
6. Dutta, D.; Naiyer, S.; Mansuri, S.; Soni, N.; Singh, V.; Bhat, K.H.; Singh, N.; Arora, G.; Mansuri, M.S. COVID-19 Diagnosis: A Comprehensive Review of the RT-QPCR Method for Detection of SARS-CoV-2. *Diagnostics* **2022**, *12*, 1503. [[CrossRef](#)] [[PubMed](#)]
7. Adnan, N.; Khandker, S.S.; Haq, A.; Chaity, M.A.; Khalek, A.; Nazim, A.Q.; Kaitsuka, T.; Tomizawa, K.; Mie, M.; Kobatake, E.; et al. Detection of SARS-CoV-2 by Antigen ELISA Test Is Highly Swayed by Viral Load and Sample Storage Condition. *Expert Rev. Anti. Infect. Ther.* **2022**, *20*, 473–481. [[CrossRef](#)] [[PubMed](#)]
8. Hui, T.C.H.; Khoo, H.W.; Young, B.E.; Mohideen, S.M.H.; Lee, Y.S.; Lim, C.J.; Leo, Y.S.; Kaw, G.J.L.; Lye, D.C.; Tan, C.H. Clinical Utility of Chest Radiography for Severe COVID-19. *Quant. Imaging Med. Surg.* **2020**, *10*, 1540–1550. [[CrossRef](#)] [[PubMed](#)]
9. Sharif, P.M.; Nematizadeh, M.; Saghazadeh, M.; Saghazadeh, A.; Rezaei, N. Computed Tomography Scan in COVID-19: A Systematic Review and Meta-Analysis. *Pol. J. Radiol.* **2022**, *87*, e1–e23. [[CrossRef](#)]
10. Oliveira, M.C.; Scharan, K.O.; Thomés, B.I.; Bernardelli, R.S.; Reese, F.B.; Kozesinski-Nakatani, A.C.; Martins, C.C.; Lobo, S.M.A.; Réa-Neto, Á. Diagnostic Accuracy of a Set of Clinical and Radiological Criteria for Screening of COVID-19 Using RT-PCR as the Reference Standard. *BMC Pulm. Med.* **2023**, *23*, 81. [[CrossRef](#)] [[PubMed](#)]
11. Filchakova, O.; Dossym, D.; Ilyas, A.; Kuanysheva, T.; Abdizhamil, A.; Bukasov, R. Review of COVID-19 Testing and Diagnostic Methods. *Talanta* **2022**, *244*, 123409. [[CrossRef](#)]
12. Mariani, S.; Minunni, M. Surface Plasmon Resonance Applications in Clinical Analysis. *Anal. Bioanal. Chem.* **2014**, *406*, 2303–2323. [[CrossRef](#)]
13. Huo, Z.; Li, Y.; Chen, B.; Zhang, W.; Yang, X.; Yang, X. Recent Advances in Surface Plasmon Resonance Imaging and Biological Applications. *Talanta* **2023**, *255*, 124213. [[CrossRef](#)]
14. Pandey, P.S.; Raghuwanshi, S.K.; Shadab, A.; Ansari, M.T.I.; Tiwari, U.K.; Kumar, S. SPR Based Biosensing Chip for COVID-19 Diagnosis—A Review. *IEEE Sens. J.* **2022**, *22*, 13800–13810. [[CrossRef](#)]
15. Syed Nor, S.N.; Rasanang, N.S.; Karman, S.; Zaman, W.S.W.K.; Harun, S.W.; Arof, H. A Review: Surface Plasmon Resonance-Based Biosensor for Early Screening of SARS-CoV2 Infection. *IEEE Access* **2022**, *10*, 1228–1244. [[CrossRef](#)]
16. Mauriz, E.; Lechuga, L.M. Current Trends in Spr Biosensing of SARS-CoV-2 Entry Inhibitors. *Chemosensors* **2021**, *9*, 330. [[CrossRef](#)]
17. Wei, H.; Zhang, C.; Du, X.; Zhang, Z. Research Progress of Biosensors for Detection of SARS-CoV-2 Variants Based on ACE2. *Talanta* **2023**, *251*, 123813. [[CrossRef](#)] [[PubMed](#)]
18. Gul, I.; Zhai, S.; Zhong, X.; Chen, Q.; Yuan, X.; Du, Z.; Chen, Z.; Raheem, M.A.; Deng, L.; Leeansyah, E.; et al. Angiotensin-Converting Enzyme 2-Based Biosensing Modalities and Devices for Coronavirus Detection. *Biosensors* **2022**, *12*, 984. [[CrossRef](#)] [[PubMed](#)]

19. Ratswohl, C.; Vázquez García, C.; Ahmad, A.U.W.; Gonschior, H.; Lebedin, M.; Silvis, C.E.; Spatt, L.; Gerhard, C.; Lehmann, M.; Sander, L.E.; et al. A Design Strategy to Generate a SARS-CoV-2 RBD Vaccine That Abrogates ACE2 Binding and Improves Neutralizing Antibody Responses. *Eur. J. Immunol.* **2023**, *53*, e2350408. [[CrossRef](#)] [[PubMed](#)]
20. Damborský, P.; Švitel, J.; Katrlík, J. Optical Biosensors. *Essays Biochem.* **2016**, *60*, 91–100. [[CrossRef](#)] [[PubMed](#)]
21. Eddin, F.B.K.; Fen, Y.W. The Principle of Nanomaterials Based Surface Plasmon Resonance Biosensors and Its Potential for Dopamine Detection. *Molecules* **2020**, *25*, 2769. [[CrossRef](#)]
22. Sharma, A.K.; Jha, R.; Gupta, B.D. Fiber-Optic Sensors Based on Surface Plasmon Resonance: A Comprehensive Review. *IEEE Sens. J.* **2007**, *7*, 1118–1129. [[CrossRef](#)]
23. Nurrohman, D.T.; Chiu, N.-F. Surface Plasmon Resonance Biosensor Performance Analysis on 2D Material Based on Graphene and Transition Metal Dichalcogenides. *ECS J. Solid State Sci. Technol.* **2020**, *9*, 115023. [[CrossRef](#)]
24. Das, C.M.; Yang, F.; Yang, Z.; Liu, X.; Hoang, Q.T.; Xu, Z.; Neermunda, S.; Kong, K.V.; Ho, H.P.; Ju, L.A.; et al. Computational Modeling for Intelligent Surface Plasmon Resonance Sensor Design and Experimental Schemes for Real-Time Plasmonic Biosensing: A Review. *Adv. Theory Simul.* **2023**, *6*, 2200886. [[CrossRef](#)]
25. D'Agata, R.; Bellassai, N.; Jungbluth, V.; Spoto, G. Recent Advances in Antifouling Materials for Surface Plasmon Resonance Biosensing in Clinical Diagnostics and Food Safety. *Polymers* **2021**, *13*, 1929. [[CrossRef](#)]
26. Daniyal, W.M.E.M.M.; Fen, Y.W.; Fauzi, N.I.M.; Hashim, H.S.; Ramdzan, N.S.M.; Omar, N.A.S. Recent Advances in Surface Plasmon Resonance Optical Sensors for Potential Application in Environmental Monitoring. *Sens. Mater.* **2020**, *32*, 4191–4200. [[CrossRef](#)]
27. Nurrohman, D.T.; Wang, Y.-H.; Chiu, N.-F. Exploring Graphene and MoS₂ Chips Based Surface Plasmon Resonance Biosensors for Diagnostic Applications. *Front. Chem.* **2020**, *8*, 728. [[CrossRef](#)]
28. Chiu, N.F.; Kuo, C.T.; Lin, T.L.; Chang, C.C.; Chen, C.Y. Ultra-High Sensitivity of the Non-Immunological Affinity of Graphene Oxide-Peptide-Based Surface Plasmon Resonance Biosensors to Detect Human Chorionic Gonadotropin. *Biosens. Bioelectron.* **2017**, *94*, 351–357. [[CrossRef](#)] [[PubMed](#)]
29. Chiu, N.F.; Tai, M.J.; Nurrohman, D.T.; Lin, T.L.; Wang, Y.H.; Chen, C.Y. Immunoassay-Amplified Responses Using a Functionalized MoS₂-Based SPR Biosensor to Detect Papp-A2 in Maternal Serum Samples to Screen for Fetal down's Syndrome. *Int. J. Nanomed.* **2021**, *16*, 2715–2733. [[CrossRef](#)]
30. Murali, S.; Rustandi, R.R.; Zheng, X.; Payne, A.; Shang, L. Applications of Surface Plasmon Resonance and Biolayer Interferometry for Virus–Ligand Binding. *Viruses* **2022**, *14*, 717. [[CrossRef](#)]
31. Kausaite-Minkstimiene, A.; Popov, A.; Ramanaviciene, A. Ultra-Sensitive SPR Immunosensors: A Comprehensive Review of Labeling and Interface Modification Using Nanostructures. *TrAC-Trends Anal. Chem.* **2024**, *170*, 117468. [[CrossRef](#)]
32. Vachali, P.P.; Li, B.; Bartschi, A.; Bernstein, P.S. Surface Plasmon Resonance (SPR)-Based Biosensor Technology for the Quantitative Characterization of Protein-Carotenoid Interactions. *Arch. Biochem. Biophys.* **2015**, *572*, 66–72. [[CrossRef](#)]
33. Sparks, R.P.; Jenkins, J.L.; Fratti, R. Use of Surface Plasmon Resonance (SPR) to Determine Binding Affinities and Kinetic Parameters Between Components Important in Fusion Machinery. In *Methods in Molecular Biology*; Fratti, R., Ed.; Springer New York: New York, NY, USA, 2019; Volume 1860, pp. 199–210. ISBN 978-1-4939-8759-7.
34. Dorozinska, H.V.; Turu, T.A.; Markina, O.M.; Dorozinsky, G.V.; Maslov, V.P. Influence of Temperature on the Measuring Accuracy of Devices Based on Surface Plasmon Resonance Phenomenon. *Mod. Instrum.* **2018**, *7*, 1–10. [[CrossRef](#)]
35. Ritzefeld, M.; Sewald, N. Real-Time Analysis of Specific Protein-DNA Interactions with Surface Plasmon Resonance. *J. Amino Acids* **2012**, *2012*, 1–19. [[CrossRef](#)] [[PubMed](#)]
36. Hahnefeld, C.; Drewianka, S.; Herberg, F.W. Determination of Kinetic Data Using Surface Plasmon Resonance Biosensors. In *Molecular Diagnosis of Infectious Diseases*; Humana Press: Totowa, NJ, USA, 2004; Volume 94, pp. 299–320.
37. Chiu, N.F.; Huang, T.Y.; Lai, H.C.; Liu, K.C. Graphene Oxide-Based SPR Biosensor Chip for Immunoassay Applications. *Nanoscale Res. Lett.* **2014**, *9*, 445. [[CrossRef](#)] [[PubMed](#)]
38. Trabucchi, A.; Iacono, R.F.; Guerra, L.L.; Faccinetti, N.I.; Krochik, A.G.; Arriazu, M.C.; Poskus, E.; Valdez, S.N. Characterization of Insulin Antibodies by Surface Plasmon Resonance in Two Clinical Cases: Brittle Diabetes and Insulin Autoimmune Syndrome. *PLoS ONE* **2013**, *8*, e84099. [[CrossRef](#)] [[PubMed](#)]
39. Hao, Y.; Yang, H.S.; Karbaschi, M.; Racine-Brzostek, S.E.; Li, P.; Zuk, R.; Yang, Y.J.; Klasse, P.J.; Shi, Y.; Zhao, Z. Measurements of SARS-CoV-2 Antibody Dissociation Rate Constant by Chaotrope-Free Biolayer Interferometry in Serum of COVID-19 Convalescent Patients. *Biosens. Bioelectron.* **2022**, *209*, 114237. [[CrossRef](#)] [[PubMed](#)]
40. Maros, H.; Juniar, S. *Handbook of Surface Plasmon Resonance*; Schasfoort, R.B.M., Ed.; Royal Society of Chemistry: Cambridge, UK, 2017; ISBN 978-1-78262-730-2.
41. Ezzati Nazhad Dolatabadi, J.; de la Guardia, M. Tips on Ligand Immobilization and Kinetic Study Using Surface Plasmon Resonance. *BioImpacts* **2016**, *6*, 117–118. [[CrossRef](#)] [[PubMed](#)]
42. Healthcare, G.E. *Biacore Sensor Surface Handbook*; Biacore: Uppsala, Sweden, 2008; Volume BR-1005-71.
43. Lan, J.; Ge, J.; Yu, J.; Shan, S.; Zhou, H.; Fan, S.; Zhang, Q.; Shi, X.; Wang, Q.; Zhang, L.; et al. Structure of the SARS-CoV-2 Spike Receptor-Binding Domain Bound to the ACE2 Receptor. *Nature* **2020**, *581*, 215–220. [[CrossRef](#)] [[PubMed](#)]
44. Rahman, M.M. Progress in Electrochemical Biosensing of SARS-CoV-2 Virus for COVID-19 Management. *Chemosensors* **2022**, *10*, 287. [[CrossRef](#)]

45. Taha, B.A.; Al-Jubouri, Q.; Al Mashhadany, Y.; Zan, M.S.D.B.; Bakar, A.A.A.; Fadhel, M.M.; Arsad, N. Photonics Enabled Intelligence System to Identify SARS-CoV-2 Mutations. *Appl. Microbiol. Biotechnol.* **2022**, *106*, 3321–3336. [[CrossRef](#)]
46. Van Vo, G.; Bagyinszky, E.; An, S.S.A. COVID-19 Genetic Variants and Their Potential Impact in Vaccine Development. *Microorganisms* **2022**, *10*, 598. [[CrossRef](#)]
47. Mohammadi, M.; Shayestehpour, M.; Mirzaei, H. The Impact of Spike Mutated Variants of SARS-CoV-2 [Alpha, Beta, Gamma, Delta, and Lambda] on the Efficacy of Subunit Recombinant Vaccines. *Braz. J. Infect. Dis.* **2021**, *25*, 101606. [[CrossRef](#)] [[PubMed](#)]
48. Xi, H.; Jiang, H.; Juhas, M.; Zhang, Y. Multiplex Biosensing for Simultaneous Detection of Mutations in SARS-CoV-2. *ACS Omega* **2021**, *6*, 25846–25859. [[CrossRef](#)]
49. Zhang, L.; Jackson, C.B.; Mou, H.; Ojha, A.; Peng, H.; Quinlan, B.D.; Rangarajan, E.S.; Pan, A.; Vanderheiden, A.; Suthar, M.S.; et al. SARS-CoV-2 Spike-Protein D614G Mutation Increases Virion Spike Density and Infectivity. *Nat. Commun.* **2020**, *11*, 6013. [[CrossRef](#)] [[PubMed](#)]
50. McLean, G.; Kamil, J.; Lee, B.; Moore, P.; Schulz, T.F.; Muik, A.; Sahin, U.; Türeci, Ö.; Pather, S. The Impact of Evolving SARS-CoV-2 Mutations and Variants on COVID-19 Vaccines. *MBio* **2022**, *13*, e02979-21. [[CrossRef](#)] [[PubMed](#)]
51. Ghoula, M.; Deyawe Kongmeneck, A.; Eid, R.; Camproux, A.C.; Moroy, G. Comparative Study of the Mutations Observed in the SARS-CoV-2 RBD Variants of Concern and Their Impact on the Interaction with the ACE2 Protein. *J. Phys. Chem. B* **2023**, *127*, 8586–8602. [[CrossRef](#)]
52. Lee, J.H.; Lee, Y.; Lee, S.K.; Kim, J.; Lee, C.S.; Kim, N.H.; Kim, H.G. Versatile Role of ACE2-Based Biosensors for Detection of SARS-CoV-2 Variants and Neutralizing Antibodies. *Biosens. Bioelectron.* **2022**, *203*, 114034. [[CrossRef](#)] [[PubMed](#)]
53. Drobysh, M.; Liustrovaite, V.; Kanetski, Y.; Brasiunas, B.; Zvirbliene, A.; Rimkute, A.; Gudas, D.; Kucinskaite-Kodze, I.; Simanavicius, M.; Ramanavicius, S.; et al. Electrochemical Biosensing Based Comparative Study of Monoclonal Antibodies against SARS-CoV-2 Nucleocapsid Protein. *Sci. Total Environ.* **2024**, *908*, 168154. [[CrossRef](#)]
54. Zhang, Y.; Juhas, M.; Kwok, C.K. Aptamers Targeting SARS-CoV-2: A Promising Tool to Fight against COVID-19. *Trends Biotechnol.* **2023**, *41*, 528–544. [[CrossRef](#)]
55. Kumar, T.H.V.; Srinivasan, S.; Krishnan, V.; Vaidyanathan, R.; Babu, K.A.; Natarajan, S.; Veerapandian, M. Peptide-Based Direct Electrochemical Detection of Receptor Binding Domains of SARS-CoV-2 Spike Protein in Pristine Samples. *Sensors Actuators B Chem.* **2023**, *377*, 133052. [[CrossRef](#)]
56. Masterson, A.N.; Muhoberac, B.B.; Gopinadhan, A.; Wilde, D.J.; Deiss, F.T.; John, C.C.; Sardar, R. Multiplexed and High-Throughput Label-Free Detection of RNA/Spike Protein/IgG/IgM Biomarkers of SARS-CoV-2 Infection Utilizing Nanoplasmonic Biosensors. *Anal. Chem.* **2021**, *93*, 8754–8763. [[CrossRef](#)]
57. Liu, Y.; Qin, Z.; Jia, X.; Zhou, J.; Li, H.; Wang, X.; Chen, Y.; Deng, J.; Jin, Z.; Wang, G. Directly and Ultrasensitivity Detecting SARS-CoV-2 Spike Protein in Pharyngeal Swab Solution by Using SERS-Based Biosensor. *Spectrochim. Acta-Part A Mol. Biomol. Spectrosc.* **2023**, *303*, 123275. [[CrossRef](#)]
58. Hao, X.; St-Pierre, J.P.; Zou, S.; Cao, X. Localized Surface Plasmon Resonance Biosensor Chip Surface Modification and Signal Amplifications toward Rapid and Sensitive Detection of COVID-19 Infections. *Biosens. Bioelectron.* **2023**, *236*, 115421. [[CrossRef](#)]
59. Wu, Q.; Wu, W.; Chen, F.; Ren, P. Highly Sensitive and Selective Surface Plasmon Resonance Biosensor for the Detection of SARS-CoV-2 Spike S1 Protein. *Analyst* **2022**, *147*, 2809–2818. [[CrossRef](#)] [[PubMed](#)]
60. Dai, Z.; Xu, X.; Wang, Y.; Li, M.; Zhou, K.; Zhang, L.; Tan, Y. Surface Plasmon Resonance Biosensor with Laser Heterodyne Feedback for Highly-Sensitive and Rapid Detection of COVID-19 Spike Antigen. *Biosens. Bioelectron.* **2022**, *206*, 114163. [[CrossRef](#)]
61. Bae, M.; Choi, S.; Kim, J.; Seo, G.; Lee, Y.W. Temperature-Insensitive Label-Free SARS-CoV-2 Spike Protein Detection Based on Complementary Refractive Index and Temperature Dependence of Multi-Mode Interference and Grating Resonance. *Talanta* **2024**, *266*, 125091. [[CrossRef](#)] [[PubMed](#)]
62. Zhang, M.; Li, X.; Pan, J.; Zhang, Y.; Zhang, L.; Wang, C.; Yan, X.; Liu, X.; Lu, G. Ultrasensitive Detection of SARS-CoV-2 Spike Protein in Untreated Saliva Using SERS-Based Biosensor. *Biosens. Bioelectron.* **2021**, *190*, 113421. [[CrossRef](#)] [[PubMed](#)]
63. Bistaffa, M.J.; Camacho, S.A.; Pazin, W.M.; Constantino, C.J.L.; Oliveira, O.N.; Aoki, P.H.B. Immunoassay Platform with Surface-Enhanced Resonance Raman Scattering for Detecting Trace Levels of SARS-CoV-2 Spike Protein. *Talanta* **2022**, *244*, 123381. [[CrossRef](#)] [[PubMed](#)]
64. Chang, T.C.; Sun, A.Y.; Huang, Y.C.; Wang, C.H.; Wang, S.C.; Chau, L.K. Integration of Power-Free and Self-Contained Microfluidic Chip with Fiber Optic Particle Plasmon Resonance Aptasensor for Rapid Detection of SARS-CoV-2 Nucleocapsid Protein. *Biosensors* **2022**, *12*, 785. [[CrossRef](#)] [[PubMed](#)]
65. Gheware, A.; Ray, A.; Rana, D.; Bajpai, P.; Nambirajan, A.; Arulselvi, S.; Mathur, P.; Tripathi, A.; Arava, S.; Das, P.; et al. ACE2 Protein Expression in Lung Tissues of Severe COVID-19 Infection. *Sci. Rep.* **2022**, *12*, 4058. [[CrossRef](#)] [[PubMed](#)]
66. Liu, L.; Chopra, P.; Li, X.; Bouwman, K.M.; Tompkins, S.M.; Wolfert, M.A.; de Vries, R.P.; Boons, G.-J. Heparan Sulfate Proteoglycans as Attachment Factor for SARS-CoV-2. *ACS Cent. Sci.* **2021**, *7*, 1009–1018. [[CrossRef](#)] [[PubMed](#)]
67. Wrapp, D.; Wang, N.; Corbett, K.S.; Goldsmith, J.A.; Hsieh, C.L.; Abiona, O.; Graham, B.S.; McLellan, J.S. Cryo-EM Structure of the 2019-nCoV Spike in the Prefusion Conformation. *Science* **2020**, *367*, 1260–1263. [[CrossRef](#)]
68. Glycoprotein, C.-S.; Walls, A.C.; Park, Y.; Tortorici, M.A.; Wall, A.; McGuire, A.T.; Veersler, D.; Walls, A.C.; Park, Y.; Tortorici, M.A.; et al. Structure, Function, and Antigenicity of the SARS-CoV-2 Spike Glycoprotein. *Cell* **2020**, *181*, 281–292.e6.
69. Yurkovetskiy, L.; Wang, X.; Pascal, K.E.; Tomkins-Tinch, C.; Nyalile, T.P.; Wang, Y.; Baum, A.; Diehl, W.E.; Dauphin, A.; Carbone, C.; et al. Structural and Functional Analysis of the D614G SARS-CoV-2 Spike Protein Variant. *Cell* **2020**, *183*, 739–751.e8. [[CrossRef](#)]

70. Xue, T.; Wu, W.; Guo, N.; Wu, C.; Huang, J.; Lai, L.; Liu, H.; Li, Y.; Wang, T.; Wang, Y. Single Point Mutations Can Potentially Enhance Infectivity of SARS-CoV-2 Revealed by: In Silico Affinity Maturation and SPR Assay. *RSC Adv.* **2021**, *11*, 14737–14745. [[CrossRef](#)]
71. Barton, M.I.; Macgowan, S.; Kutuzov, M.; Dushek, O.; Barton, G.J.; Anton Van Der Merwe, P. Effects of Common Mutations in the Sars-Cov-2 Spike Rbd and Its Ligand the Human Ace2 Receptor on Binding Affinity and Kinetics. *eLife* **2021**, *10*, e70658. [[CrossRef](#)] [[PubMed](#)]
72. Fratev, F. R346K Mutation in the Mu Variant of SARS-CoV-2 Alters the Interactions with Monoclonal Antibodies from Class 2: A Free Energy Perturbation Study. *J. Chem. Inf. Model.* **2022**, *62*, 627–631. [[CrossRef](#)]
73. Aggarwal, A.; Naskar, S.; Maroli, N.; Gorai, B.; Dixit, N.M.; Maiti, P.K. Mechanistic Insights into the Effects of Key Mutations on SARS-CoV-2 RBD-ACE2 Binding. *Phys. Chem. Chem. Phys.* **2021**, *23*, 26451–26458. [[CrossRef](#)]
74. Taft, J.M.; Weber, C.R.; Gao, B.; Ehling, R.A.; Han, J.; Frei, L.; Metcalfe, S.W.; Overath, M.D.; Yermanos, A.; Kelton, W.; et al. Deep Mutational Learning Predicts ACE2 Binding and Antibody Escape to Combinatorial Mutations in the SARS-CoV-2 Receptor-Binding Domain. *Cell* **2022**, *185*, 4008–4022.e14. [[CrossRef](#)]
75. Chen, C.; Boorla, V.S.; Banerjee, D.; Chowdhury, R.; Cavener, V.S.; Nissly, R.H.; Gontu, A.; Boyle, N.R.; Vandegrift, K.; Nair, M.S.; et al. Computational Prediction of the Effect of Amino Acid Changes on the Binding Affinity between SARS-CoV-2 Spike RBD and Human ACE2. *Proc. Natl. Acad. Sci. USA* **2021**, *118*, e2106480118. [[CrossRef](#)] [[PubMed](#)]
76. Barnes, J.E.; Lund-Andersen, P.K.; Patel, J.S.; Ytreberg, F.M. The Effect of Mutations on Binding Interactions between the SARS-CoV-2 Receptor Binding Domain and Neutralizing Antibodies B38 and CB6. *Sci. Rep.* **2022**, *12*, 18819. [[CrossRef](#)] [[PubMed](#)]
77. Leonard, A.C.; Weinstein, J.J.; Steiner, P.J.; Erbse, A.H.; Fleishman, S.J.; Whitehead, T.A. Stabilization of the SARS-CoV-2 Receptor Binding Domain by Protein Core Redesign and Deep Mutational Scanning. *Protein Eng. Des. Sel.* **2022**, *35*, gzac002. [[CrossRef](#)] [[PubMed](#)]
78. Sergeeva, A.P.; Katsamba, P.S.; Liao, J.; Sampson, J.M.; Bahna, F.; Mannepalli, S.; Morano, N.C.; Shapiro, L.; Friesner, R.A.; Honig, B. Free Energy Perturbation Calculations of Mutation Effects on SARS-CoV-2 RBD::ACE2 Binding Affinity. *J. Mol. Biol.* **2023**, *435*, 168187. [[CrossRef](#)] [[PubMed](#)]
79. Makowski, E.K.; Schardt, J.S.; Smith, M.D.; Tessier, P.M. Mutational Analysis of SARS-CoV-2 Variants of Concern Reveals Key Tradeoffs between Receptor Affinity and Antibody Escape. *PLoS Comput. Biol.* **2022**, *18*, e1010160. [[CrossRef](#)] [[PubMed](#)]
80. Gupta, A.K.; Hsu, C.H.; Lai, C.S. Enhancement of the Au/ZnO-NA Plasmonic SERS Signal Using Principal Component Analysis as a Machine Learning Approach. *IEEE Photonics J.* **2020**, *12*, 2200611. [[CrossRef](#)]
81. Paryanti, G.; Faig, H.; Rokach, L.; Sadot, D. A Direct Learning Approach for Neural Network Based Pre-Distortion for Coherent Nonlinear Optical Transmitter. *J. Light. Technol.* **2020**, *38*, 3883–3896. [[CrossRef](#)]
82. Williamson, I.A.D.; Hughes, T.W.; Minkov, M.; Bartlett, B.; Pai, S.; Fan, S. Tunable Nonlinear Activation Functions for Optical Neural Networks. *Opt. InfoBase Conf. Pap.* **2020**. [[CrossRef](#)]
83. Arano-Martinez, J.A.; Martínez-González, C.L.; Salazar, M.I.; Torres-Torres, C. A Framework for Biosensors Assisted by Multiphoton Effects and Machine Learning. *Biosensors* **2022**, *12*, 710. [[CrossRef](#)]
84. Qatamin, A.H.; Ghithan, J.H.; Moreno, M.; Nunn, B.M.; Jones, K.B.; Zamborini, F.P.; Keynton, R.S.; O'toole, M.G.; Mendes, S.B. Detection of Influenza Virus by Electrochemical Surface Plasmon Resonance under Potential Modulation. *Appl. Opt.* **2019**, *58*, SW4C.4. [[CrossRef](#)]
85. Song, C.; Jiang, X.; Yang, Y.; Zhang, J.; Larson, S.; Zhao, Y.; Wang, L. High-Sensitive Assay of Nucleic Acid Using Tetrahedral DNA Probes and DNA Concatamers with a Surface-Enhanced Raman Scattering/Surface Plasmon Resonance Dual-Mode Biosensor Based on a Silver Nanorod-Covered Silver Nanohole Array. *ACS Appl. Mater. Interfaces* **2020**, *12*, 31242–31254. [[CrossRef](#)] [[PubMed](#)]
86. Hasler, R.; Steger-Polt, M.H.; Reiner-Rozman, C.; Fossati, S.; Lee, S.; Aspermaier, P.; Kleber, C.; Ibáñez, M.; Dostalek, J.; Knoll, W. Optical and Electronic Signal Stabilization of Plasmonic Fiber Optic Gate Electrodes: Towards Improved Real-Time Dual-Mode Biosensing. *Front. Phys.* **2023**, *11*, 1202132. [[CrossRef](#)]
87. Caucheteur, C.; Guo, T.; Albert, J. Review of Plasmonic Fiber Optic Biochemical Sensors: Improving the Limit of Detection. *Anal. Bioanal. Chem.* **2015**, *407*, 3883–3897. [[CrossRef](#)] [[PubMed](#)]

Disclaimer/Publisher's Note: The statements, opinions and data contained in all publications are solely those of the individual author(s) and contributor(s) and not of MDPI and/or the editor(s). MDPI and/or the editor(s) disclaim responsibility for any injury to people or property resulting from any ideas, methods, instructions or products referred to in the content.